Materials Letters 221 (2018) 57–61

Contents lists available at ScienceDirect

Materials Letters

journal homepage: www.elsevier.com/locate/mlblue

Controllable assembly of sandwich-structured SnO_2/Fe_2O_3 multilayer nanosheets for high sensitive acetone detection

Junping Liu, Yanzhe Wang, Lianqiang Wang, Hongwei Tian, Yi Zeng *

College of Materials Science and Engineering, Key Laboratory of Automobile Materials of Ministry of Educations, and State Key Laboratory of Superhard Materials, Jilin University, Changchun, China

ARTICLE INFO

Article history:
Received 3 February 2018
Received in revised form 14 March 2018
Accepted 17 March 2018
Available online 17 March 2018

Keywords:
Tin oxide
Ferric oxide
Multilayered structure
Heterostructure
Gas sensor

ABSTRACT

A new type of hierarchically nonspherical architecture with sandwich-structured multilayer nanosheets has been successfully prepared via a controllable multistep approach in case of SnO_2/Fe_2O_3 heterostructures. The morphological characterization reveals that unique sandwich-structured SnO_2/Fe_2O_3 multilayer nanosheets (MNSs) are constructed via the self-assembly of densely well-aligned Fe_2O_3 nanorod layers to cover and fill the interlayers of hexagonal SnO_2 hollow multilayer nanosheets (HMNs). When used as the sensing materials for acetone detection, the sandwich hetero-nanostructures demonstrate evidently improved sensing performance compared to pure SnO_2. The significantly improved sensing performance can be attributed not only to the rational microstructures for fast transfer of gas molecules, but also to the additional effects of loaded Fe_2O_3 ultrathin nanorods.

1. Introduction

Semiconducting metal oxides, as one type of promising candidates for gas-sensing materials, have attracted tremendous attention owing to their low cost, easily tunable structural and sensing characters in detecting various target gases [1]. From the materials perspective, rational design of hierarchically porous or hollow architectures of desired candidates has been widely recognized as an effective route for the boost of their gas-sensing performances [2–4]. Beyond the strategy of optimizing material structures, hybrid-composite design is also proved to be highly desirable with respect to a dramatic improvement in the sensing performances in virtue of tunable composition and synergistic effect. In the case of n-type semiconducting oxides, tin dioxide (SnO_2) has long been applied as an appealing sensing material with various shapes in detecting diverse gas species [5–9]. In the past few years, broadening the sensing materials from single-component SnO_2 to SnO_2 matrix heterostructures, such as SnO_2/Au, SnO_2/Pd, SnO_2/ZnO, SnO_2/Fe_2O_3, SnO_2/TiO_2, and so on [10–14], has received more attention and significantly improved the performances. Despite considerable efforts being dedicated to integrate the fascinating merits of proper configuration and synergistic contribution, facile assembly of heterogeneous low-dimensional subunits on another oxide matrix often encounters the compatibility issue, and in fact the resulting heterostructures are usually degraded to dense-agglomerated form. Understanding key factors for constructing heterogeneous oxides with desired porous architecture by a simple and economical route still remains challenging yet highly desirable.

In this work, we present a multistep route for unique sandwich-structured SnO_2/Fe_2O_3 MNSs through covering ultrathin Fe_2O_3 nanorod-assembled layers on all surfaces of hexagonal SnO_2 HMNs. The morphology and microstructure of as-obtained SnO_2/Fe_2O_3 MNSs are examined. Benefitting from the porous feature and highly interconnected heterogeneous interfaces of SnO_2/Fe_2O_3 MNSs, the improved gas-sensing performances of the obtained SnO_2/Fe_2O_3 MNSs can be anticipated.

2. Experimental

All the chemical reagents are of analytical grade as purchased from Sinopharm Chemical Reagent Co. Ltd (China) and used without further purification. The route for SnO_2 HMNs is according to our previous report with some modifications [15]. As for the final SnO_2/Fe_2O_3 MNSs, the as-obtained SnO_2 (20 mg) was dispersed into 40 mL of aqueous solution, including $Na_2SO_4{\cdot}10H_2O$ (85.8 mg) and $FeCl_3{\cdot}6H_2O$ (71.6 mg). After stirring for 10 min, this suspension was transferred into a Teflon-lined stainless steel autoclave, sealed tightly, and then maintained at 120 °C for 2 h. After cooled naturally down to room temperature, the dark-red precipitates were centrifugally separated, washed with absolute

* Corresponding author.
E-mail address: zengyi@jlu.edu.cn (Y. Zeng).

https://doi.org/10.1016/j.matlet.2018.03.084
0167-577X/

ethanol/DI water for several times, and dried at 60 °C overnight. Finally, the precipitates were annealed at 450 °C for 2 h with a ramping rate of 5 °C min^{-1} to obtain the final SnO_2/Fe_2O_3 MNSs.

The crystal structure and morphology of the samples were characterized by X-ray diffraction (XRD, Bruke D8 Advance) with Cu Kα radiation, field emission scanning electron microscopy (FESEM, JEOL JSM-6700F), transmission electron microscopy (TEM), selected area electron diffraction (SAED), and high-resolution transmission electron microscopy (HRTEM, JEOL JEM-2100F). The detailed process of sensor fabrication was described in our previous reports [11]. The response (R) is defined as the ratio of the resistance of the sensor in dry air (R_a) to that in target gases (R_g). The response and recovery time (τ_{res} and τ_{recov}) are defined as the time taken by the sensor to achieve 90% of the total resistance change in the case of adsorption and desorption, respectively.

3. Results and discussion

The phase purity and structure of the as-obtained samples after different steps were firstly characterized via XRD measurement. As can be seen in Fig. 1a, all the diffraction peaks from SnO_2 sample are consistent with patterns from a standard SnO_2 rutile phase (JCPDS card no. 41-1445) and no peaks from any other impurities are identified. As for the final hydrothermal sample, besides a part of diffraction peaks are assigned to tetragonal SnO_2 phase, the residual peaks can be discerned to well match with the standard pattern from the rhombohedral α-Fe_2O_3 (JCPDS card no. 33-0664). It demonstrates that the final samples are constructed by two mixed crystalline phases of SnO_2 and Fe_2O_3. The morphological and structural characters of the as-prepared SnO_2 and SnO_2/Fe_2O_3 samples are also examined, respectively. Fig. 1b confirms that the obtained SnO_2 sample is composed of flowerlike aggregated nanosheets with coarse surfaces and partly cracked laterals (indicated by white arrow). More importantly, the unique hollow interior and multilayered structure of SnO_2 nanosheets are identified through the relatively light contrast between the dark outlines and multiple pale/dark strips from their side projections (Fig. 1c). The inset SAED pattern and HRTEM image (Fig. 1d) presents that polycrystalline SnO_2 nanosheets are assembled by primary nanoparticles with diameter of around 5 nm and the obvious spaces among nanoparticles confirm the highly porous merit (indicated by white arrow), which can guarantee the effective diffusion of gas molecules during the sensing process.

A low-magnification image (Fig. 2a) indicates that SnO_2/Fe_2O_3 samples generally maintain the basic shape and size of SnO_2 HMNs. Evidently, numerous Fe_2O_3 outshoots are homogenously distributed on surfaces of SnO_2 nanosheet to form more rougher and hairy appearance. As shown in Fig. 2b, these Fe_2O_3 rod-like primary building blocks with almost uniform diameter stand nearly perpendicularly on all the surfaces of different SnO_2 layers to form the so-called sandwich-like structure of SnO_2/Fe_2O_3 MNSs. The local enlarged TEM image (Fig. 2c) clearly displays that the average length of Fe_2O_3 primary nanorods is about 160 nm and the outmost layer assembled from well-aligned Fe_2O_3 primary nanorods is merged well with SnO_2 layer (with outer Fe_2O_3 and inner SnO_2 layers indicated by arrows). A slight deviation from 90° should be ascribed mainly to the jostle among the densely arranged primary

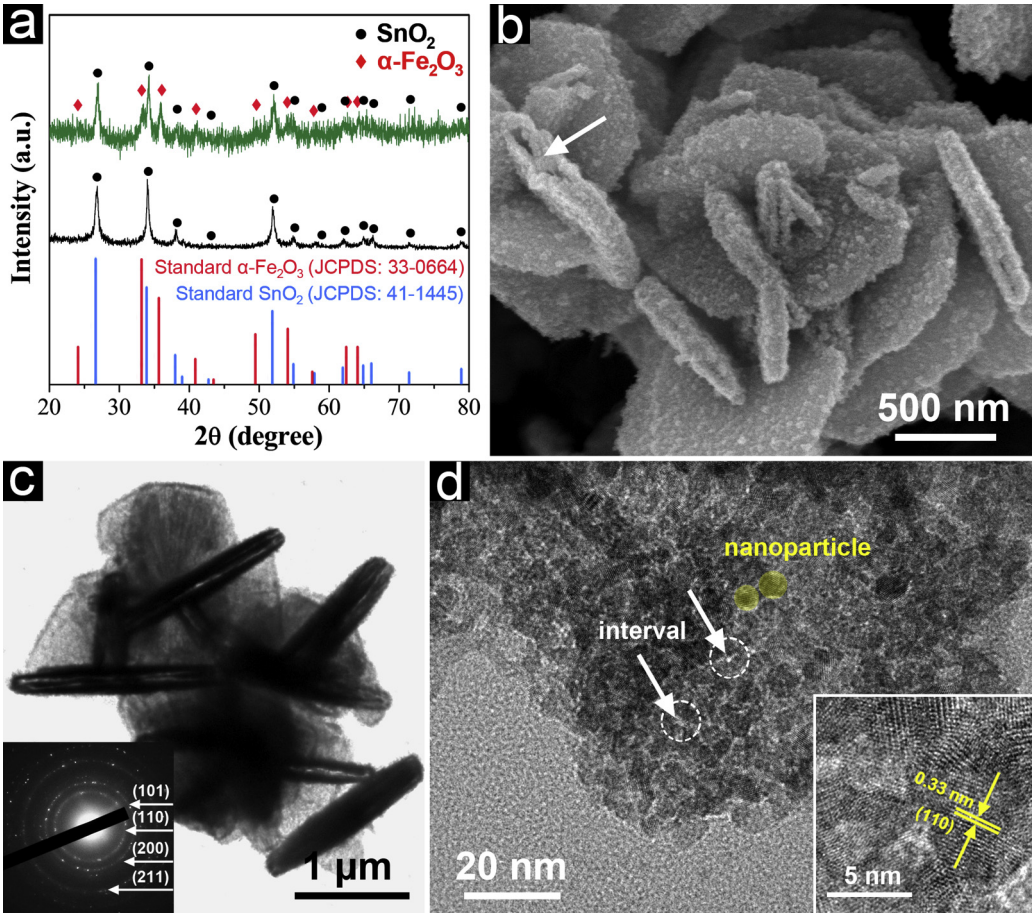

Fig. 1. XRD pattern of SnO_2 HMNs and SnO_2/Fe_2O_3 MNSs (a); typical FESEM (b), TEM (c) and HRTEM (d) images of SnO_2 HMNs. The inset of Fig. 1c is a SAED pattern.